A Schamel equation for ion acoustic waves in superthermal plasmas

G. Williams *
Centre for Plasma Physics, Department of Physics and Astronomy, Queen's University Belfast, BT7 1NN, Northern Ireland, UK

F. Verheest
Sterrenkundig Observatorium, Universiteit Gent, Krijgslaan 281, B-9000 Gent, Belgium, and School of Chemistry and Physics, University of KwaZulu-Natal, Durban 4000, South Africa

M. A. Hellberg
School of Chemistry and Physics, University of KwaZulu-Natal, Durban 4000, South Africa

M. G. M. Anowar
Department of Physics, Begum Rokeya University, Rangpur, Rangpur-5400, Bangladesh

I. Kourakis
Queen's University Belfast, Centre for Plasma Physics, Department of Physics and Astronomy, BT7 1NN, Northern Ireland, UK
(Dated: June 27, 2014)

An investigation of the propagation of ion acoustic waves in nonthermal plasmas in the presence of trapped electrons has been undertaken. This has been motivated by space and laboratory plasma observations of plasmas containing energetic particles, resulting in long-tailed distributions, in combination with trapped particles, whereby some of the plasma particles are confined to a finite region of phase space. An unmagnetized collisionless electron-ion plasma is considered, featuring a non-Maxwellian-trapped electron distribution, which is modelled by a kappa distribution function combined with a Schamel distribution. The effect of particle trapping has been considered, resulting in an expression for the electron density. Reductive perturbation theory has been used to construct a KdV-like Schamel equation, and examine its behaviour. A solitary wave solution is presented and its dynamics discussed. The chief modification due to the presence of particle trapping is stronger nonlinearity, while enhanced superthermality affects the amplitude and width of solitons with a fixed value of incremental soliton speed adversely.

I. INTRODUCTION

The presence of energetic superthermal particles in plasmas, resulting in long-tailed distributions, is an intrinsic element in many space and laboratory plasma observations. Many different models have been proposed to describe this effect on wave dynamics via phenomenological modification to the electron distribution function.

One approach to non-Maxwellian plasma modelling is provided by the kappa distribution [1–3], which was introduced by Vasyliunas [1] to fit phenomenologically the power law-like dependence of electron distribution functions observed in space. The spectral index, kappa (κ), for which the kappa distribution is named, acts to modify the effective thermal speed in the distribution function. At low values of κ, distributions exhibit strong superthermality - by this we mean that there is an excess in the superthermal component of the distribution compared to that of a Maxwellian. At very large values of kappa, the distribution function approaches a Maxwellian distribution. It is commonly fitted to observational data [2, 4, 5]. Interestingly, it has been argued that the kappa scenario derives from the Tsallis distribution [6, 7], although this speculative analogy is rather phenomenological and remains the subject of debate [2, 7]. We shall not pursue this analogy here as this is beyond our scope.

The Korteweg-de Vries (KdV) equation describes the one-dimensional, time asymptotic behaviour of weakly dispersive waves with a small but finite amplitude, and the theory has been applied to ion acoustic waves in plasmas [8, 9]. In this theory, nonlinear steepening of the wave is balanced by dispersion, and in recent years, several studies have analysed ion acoustic waves and the electrostatic structures that arise as a consequence of their dynamics in κ-distributed plasmas using the KdV theory [10, 11].

Another commonly observed phenomenon in both space and laboratory plasmas is that of particle trapping, whereby some of the plasma particles are confined to a finite region of phase space where they bounce back and forth. These have been studied numerically [12, 13], and have been observed in both space and laboratory contexts [14–18]. Cattell et al. [15] noted examples of solitary waves at the Earth's magnetopause; Ergun et

*E-mail: gwilliams06@qub.ac.uk

al. [16, 17] and Andersson et al. [18] observed electron phase-space holes in both the upward and downward current region of the aurora. In addition, many laboratory observations of the free expansion of plasma into a vacuum have recorded the propagation of holes, solitons, and rarefaction waves [19]. The nonlinear particle trapping effect was first included in analytical models of electrostatic structures by Bernstein, Greene and Kruskal (BGK) [20]. Later Schamel [21, 22] developed a pseudopotential method for the construction of equilibrium solutions, and also derived a KdV-like equation, often called the Schamel equation [23], for weakly nonlinear ion acoustic waves which are modified by the presence of trapped electrons [22]. The chief effect of the modification to the KdV equation is stronger nonlinearity. This method has later been applied to the study of non-Maxwellian dust ion acoustic waves by Pajouh and Abbasi [24].

In this paper, we seek to consider the effect of particle trapping in a κ-distributed plasma, deriving an expression for the electron density. We have used reductive perturbation theory to construct a Schamel KdV equation, and examine its dynamics. The Schamel-kappa distribution allows for the effects of trapped particles in the low energy part of the distribution, while including the usual enhanced non-Maxwellian tail, with an excess of superthermal particles, typical of a kappa distribution.

The paper is structured as follows. In Section II, we derive an expression for the electron density in a Schamel-kappa distribution. This is followed in Section III by an outline of the ion fluid model we have adopted. Section IV deals with linear ion acoustic wave analysis, and small amplitude nonlinear waves are discussed in Section V. A solitary wave solution is presented and its dynamics discussed in Section VI. This is followed by the presentation of numerical results in Section VII. We discuss our conclusions in Section VIII.

II. THE SCHAMEL-KAPPA DISTRIBUTION

The kappa electron distribution in one dimension [2] is given by:

$$f_e^\kappa(v) = \frac{N_0}{(\pi\kappa\theta^2)^{1/2}} \frac{\Gamma(\kappa)}{\Gamma(\kappa - \frac{1}{2})} \left(1 + \frac{v^2}{\kappa\theta^2}\right)^{-\kappa}, \qquad (1)$$

where N_0 is the species equilibrium number density and the effective thermal speed is

$$\theta = \left[(\kappa - 3/2)/\kappa\right]^{1/2} (2k_B T/m)^{1/2},$$

which requires $\kappa > 3/2$ to be physically realistic.

Normalizing such that $\int_{-\infty}^{+\infty} f_e^\kappa(v)dv = 1$, and using the energy conservation relation $(m_e v_e^2/2 - e\phi = m_e V^2/2$, where $e\phi$ is the increase in potential energy,

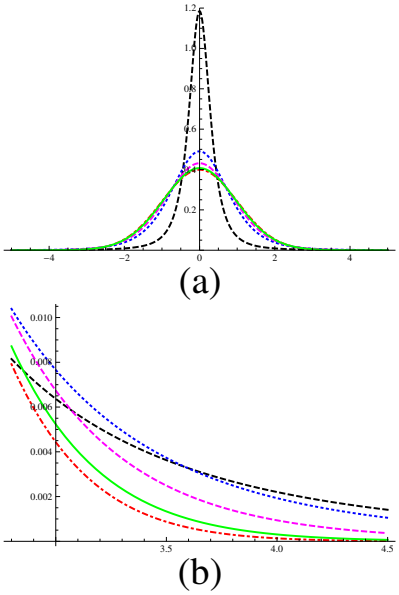

FIG. 1: (Color online). (a) and (b): Plot of the kappa distribution as given by (1) where (b) zooms in on the positive tail of the distribution. In both plots, the dashed (black) line is $\kappa = 1.6$, the dotted (blue) line is $\kappa = 3$, the dashed (mauve) line is $\kappa = 6$, the solid (green) line is $\kappa = 20$, and the dot-dashed (red) line is the Maxwellian case as $\kappa \to \infty$.

and V is the velocity of the particles in the initial equilibrium state), scaling v by $(k_B T/m)^{1/2}$, and ϕ by $k_B T/e$, Eqn. (1) can be written as:

$$f_e^\kappa(v,\phi) = \frac{1}{\sqrt{2\pi}(\kappa - \frac{3}{2})^{\frac{1}{2}}} \frac{\Gamma(\kappa)}{\Gamma(\kappa - \frac{1}{2})} \left(1 + \frac{\frac{v^2}{2} - \phi}{\kappa - \frac{3}{2}}\right)^{-\kappa}. \qquad (2)$$

Taking the limit as $\kappa \to \infty$, we get the Maxwellian distribution:

$$f_e^{Max}(v,\phi) = \frac{1}{\sqrt{2\pi}} \exp[-(v^2/2 - \phi)]. \qquad (3)$$

Figure 1 is a plot of $f_e^\kappa(v)$ for different values of κ. We can see that at lower values of κ the centre and tail of the distribution are higher; as a result there are fewer particle near the thermal speed compared with a Maxwellian distribution, if the density is constant.

Schamel [21] introduced the concept of a separatrix to the distribution which separates free electrons from trapped ones. The energy of the electrons is defined as $E_e = v(x)^2/2 - \phi(x)$, and the energy separatrix occurs at the point where the energy equals zero, that is, $E_{es} := v(x)^2/2 - \phi(x) = 0$. Wherever $E_e > 0$, electrons are free, and their distribution is given by Eqn. (3), and when $E_e < 0$ electrons are trapped. The distribution for the

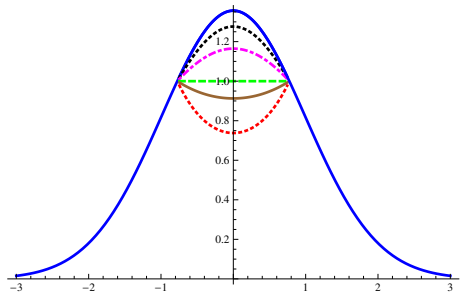

FIG. 2: (Color online). Plot of the Schamel-κ distribution incorporating trapped electrons as given by (2) and (5). The solid (blue) line represents $\beta = 1$, the dotted (black) line is $\beta = 0.8$, the dot-dashed (mauve) line is $\beta = 0.5$, the dashed (green) line is $\beta = 0$, the solid (brown) line is $\beta = -0.3$ and the dotted (red) line is $\beta = -1$. Here we have taken $\phi = 0.3$ and $\kappa = 100$.

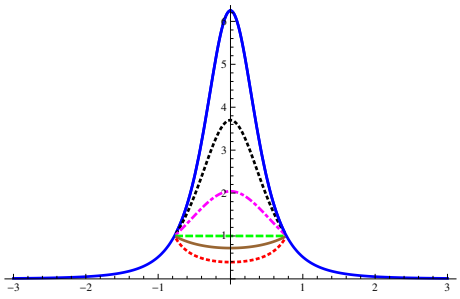

FIG. 3: (Color online). As in Fig. 2, but using $\kappa = 2$.

trapped electrons is then defined as:

$$f_{e,t}^{Max}(v,\phi) = \frac{1}{\sqrt{2\pi}} \exp[-\beta(v^2/2 - \phi)] \text{ for } E_e \leq 0, \tag{4}$$

where β is a parameter which determines the efficiency of electron trapping.

Applying the same argument for the separatrix to the kappa distribution, where Eqn. (2) applies to free κ-distributed electrons, that is, when $E_e > 0$, and for trapped electrons in a κ-distribution, when $E_e < 0$, that is, $-\sqrt{2\phi} < v < \sqrt{2\phi}$, a trapped electron κ distribution can be written as:

$$f_{e,t}^{\kappa}(v,\phi) = \frac{1}{\sqrt{2\pi}(\kappa - \frac{3}{2})^{1/2}} \frac{\Gamma(\kappa)}{\Gamma(\kappa - 1/2)} \times \left[1 + \beta \left(\frac{v^2/2 - \phi}{\kappa - \frac{3}{2}}\right)\right]^{-\kappa} \text{ for } E_e \leq 0. \tag{5}$$

Equation (5) recovers Eqn. (4) as $\kappa \to \infty$, and Eqn. (2) as $\beta \to 1$. Figures 2 and 3 show the Schamel-κ distribution for various values of β when $\kappa = 100$ (Fig. 2) and $\kappa = 2$ (Fig. 3). When $\beta = 1$, this corresponds to a kappa distribution which has no trapped electrons. As the value of β is reduced, the distribution peak is suppressed, and at $\beta = 0$, we have a flat-topped distribution. The value of β can be negative, and we see that this corresponds to a dip in the centre of the distribution. As $\beta \to -\infty$, the centre of the distribution $\to 0$. To find the electron density, we need to integrate over all v from $-\infty$ to $+\infty$.

The following integrals need to be computed:

$$n_e(\phi) = \int_{-\infty}^{-\sqrt{2\phi}} f_e^{\kappa}(v,\phi) + \int_{-\sqrt{2\phi}}^{\sqrt{2\phi}} f_{e,t}^{\kappa}(v,\phi) + \int_{\sqrt{2\phi}}^{+\infty} f_e^{\kappa}(v,\phi), \tag{6}$$

where $f_e^{\kappa}(v,\phi)$ is given by Eqn. (2), and $f_{e,t}^{\kappa}(v,\phi)$ is given by Eqn. (5). The result is:

$$\begin{aligned} n_e(\phi) = {} & (2\kappa - 3)^{\kappa - 3/2} (2\kappa - 3 - 2\phi)^{-\kappa} \\ & \times \Big[(2\kappa - 3)\sqrt{2\kappa - 3 - 2\phi} - \frac{4}{\Gamma[\kappa - 3/2]}\sqrt{2/\pi} \\ & \times \sqrt{\phi} \quad \Gamma[\kappa] \quad {}_2F_1\left[\frac{1}{2}, \kappa, \frac{3}{2}, \frac{2\phi}{3 - 2\kappa + 2\phi}\right] \Big] \\ & + \frac{2}{\Gamma[\kappa - 1/2]}\sqrt{2/\pi}\,(2\kappa - 3)^{\kappa - 1/2}\sqrt{\phi} \\ & \times (2\kappa - 3 - 2\beta\phi)^{-\kappa}\,\Gamma[\kappa] \\ & \times {}_2F_1\left[\frac{1}{2}, \kappa, \frac{3}{2}, \frac{2\beta\phi}{3 - 2\kappa + 2\beta\phi}\right]. \end{aligned} \tag{7}$$

One can demonstrate numerically that $n_e(\phi) > 0$ for all κ, β, ϕ. Taylor-expanding the expression for ϕ about 0 and truncating at 2nd order gives:

$$\begin{aligned} n_e(\phi) \simeq {} & 1 + \left(\frac{2\kappa - 1}{2\kappa - 3}\right)\phi \\ & + \frac{8\sqrt{2/\pi}(\beta - 1)\kappa\Gamma[\kappa]}{3(2\kappa - 3)^{3/2}\Gamma[\kappa - 1/2]}\phi^{3/2} + \frac{4\kappa^2 - 1}{2(2\kappa - 3)^2}\phi^2. \end{aligned} \tag{8}$$

The limit of Eqn. (8) as $\kappa \to \infty$ is given by Eqn. (9) below, which agrees with the Schamel expression for the electron density in a Maxwellian plasma [22]:

$$n_e(\phi) \simeq 1 + \phi + \frac{4(\beta - 1)}{3\sqrt{\pi}}\phi^{3/2} + \phi^2/2 + \ldots \tag{9}$$

In addition, the limit of Eqn. (8) as $\beta \to 1$ gives the electron distribution in a kappa-distributed plasma, with

no trapped electrons:

$$n_e(\phi) \simeq 1 + \left(\frac{2\kappa - 1}{2\kappa - 3}\right)\phi + \frac{4\kappa^2 - 1}{2(2\kappa - 3)^2}\phi^2, \quad (10)$$

in agreement with Eqn. (14) of Ref. 25.

III. THE FLUID MODEL

We shall now consider ion acoustic waves propagating in a plasma consisting of cold ions ($T_i = 0$) and electrons with a Schamel-kappa distribution. As is usual for ion acoustic structures, we require that the wave phase speed lies between the ion and electron thermal speeds, that is, $v_{ti} \ll v_{ph} \ll v_{te}$, to avoid Landau damping [26].

The one dimensional system of normalized fluid equations for the ions, together with Poisson's equation are:

$$\frac{\partial n}{\partial t} + \frac{\partial (nu)}{\partial x} = 0, \quad (11)$$

$$\frac{\partial u}{\partial t} + u\frac{\partial u}{\partial x} = -\frac{\partial \phi}{\partial x}, \quad (12)$$

$$\frac{\partial^2 \phi}{\partial x^2} = n_e - n \simeq -(n-1) + p\phi + q\phi^{3/2} + r\phi^2, \quad (13)$$

where n and u represent the ion density and velocity respectively, and ϕ is the electrostatic potential. We assume charge neutrality at equilibrium, that is, $n_e = Zn_0$, where Zn_0 is the equilibrium ion charge density. We have substituted the Taylor-expanded expression for the electron density n_e from Eqn. (8) into the Poisson Equation (13), with

$$p = \frac{2\kappa - 1}{2\kappa - 3}, \quad (14)$$

$$q = \frac{8\sqrt{2/\pi}(\beta - 1) \quad \kappa \quad \Gamma(\kappa)}{3(2\kappa - 3)^{3/2}\Gamma(\kappa - 1/2)} \quad (15)$$

$$r = \frac{4\kappa^2 - 1}{2(2\kappa - 3)^2} \quad (16)$$

To make the calculations tractable analytically, we have employed the following normalizations: lengths are normalized by a characteristic Debye length $\lambda_D = \left(\frac{\epsilon_0 k_B T_e}{n_0 Z e^2}\right)^{\frac{1}{2}}$, time by the inverse plasma frequency $\omega_p = \left(\frac{n_0 Z^2 e^2}{\epsilon_0 m}\right)^{\frac{1}{2}}$, number density by the equilibrium ion density n_0, electrostatic potential by $\left(\frac{k_B T_e}{e}\right)$, and velocities by a characteristic sound speed $c_s = \left(\frac{Z k_B T_e}{m}\right)^{\frac{1}{2}}$.

IV. LINEAR WAVE ANALYSIS

We can linearize the system of fluid equations in the usual way to obtain the linear dispersion equation:

$$\omega^2 = \frac{k^2}{k^2 + p}, \quad (17)$$

where p is given by Eqn. (14). From Eqn. (17), we note that p is essentially the effective inverse (square) screening length, that is, $\lambda_D = p^{-1/2}$. Importantly, this now depends on κ. This reflects the fact that energetic particles affect the Debye screening mechanism by modifying the electron cloud distribution surrounding the ions, as is well-known for waves in a kappa-distributed plasma [2]. We note that the Schamel trapping parameter β does not appear in Eqn. (17). This shows the typical behaviour of this model, viz. that the trapping does not have an effect on the linear wave. For the sake of completeness, we emphasize that it follows immediately from Eqn. (17) that the normalized phase speed of the linear wave is $p^{-1/2}$.

V. REDUCTIVE PERTURBATION THEORY

To study weakly nonlinear potential excitations, we follow the reductive perturbation technique of Schamel [22], and stretch variables as follows:

$$\zeta = \epsilon^{1/4}(x - Vt),$$
$$\tau = \epsilon^{3/4}t, \quad (18)$$

where ϵ is an infinitely small parameter. The independent variables n, u, ϕ can also be expanded in a power series (truncated to second order) of the parameter ϵ:

$$n \sim 1 + \epsilon n_1 + \epsilon^{3/2} n_2,$$
$$u \sim \epsilon u_1 + \epsilon^{3/2} u_2,$$
$$\phi \sim \epsilon \phi_1 + \epsilon^{3/2} \phi_2.$$

Substituting in Eqns. (11 - 13) and extracting the lowest order terms in ϵ, one obtains compatibility conditions:

$$-V\frac{\partial n_1}{\partial \zeta} + \frac{\partial u_1}{\partial \zeta} = 0, \quad (19)$$

$$-V\frac{\partial u_1}{\partial \zeta} + \frac{\partial \phi_1}{\partial \zeta} = 0, \quad (20)$$

$$n_1 - p\phi_1 = 0. \quad (21)$$

Combining these, we find:

$$n_1 = p^{1/2} u_1 = p\phi_1, \quad (22)$$

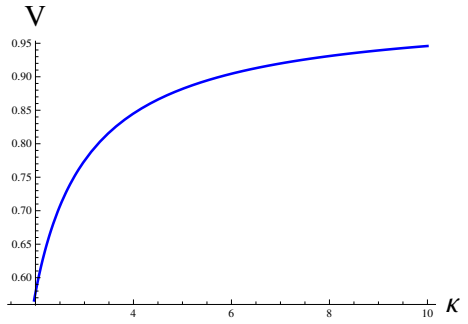

FIG. 4: (Color online). Plot of the the phase speed V vs. κ.

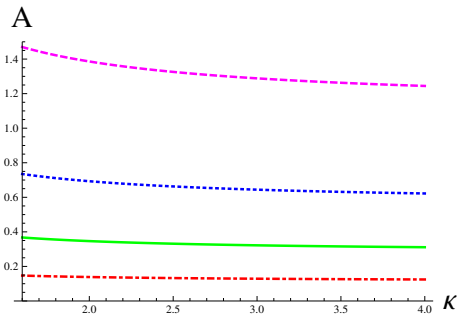

FIG. 5: (Color online). Plot of the coefficient A vs. κ. The dot-dashed (red) line represents $\beta = 0.8$, the solid (green) line is $\beta = 0.5$, the dotted (blue) line is $\beta = 0$, and the dashed (mauve) line is $\beta = -1$.

where

$$p = \frac{1}{V^2} = \frac{2\kappa - 1}{2\kappa - 3}. \tag{23}$$

V is the phase speed, and as seen in Fig. 4, it is dependent on the κ parameter, whereby increased superthermality (lower values of κ) has the effect of reducing the phase speed. The second order terms in ϵ yield:

$$-V\frac{\partial n_2}{\partial \zeta} + \frac{1}{V^2}\frac{\partial \phi_1}{\partial \tau} + \frac{\partial u_2}{\partial \zeta} = 0, \tag{24}$$

$$-V\frac{\partial u_2}{\partial \zeta} + \frac{1}{V}\frac{\partial \phi_1}{\partial \tau} + \frac{\partial \phi_2}{\partial \zeta} = 0, \tag{25}$$

$$\frac{\partial^2 \phi_1}{\partial x^2} + n_2 - \frac{1}{V^2}\phi_2 - q\phi_1^{3/2} = 0. \tag{26}$$

These compatibility conditions are combined and result in a KdV-like Schamel equation [22]:

$$\frac{\partial \phi_1}{\partial \tau} + A\phi_1^{1/2}\frac{\partial \phi_1}{\partial \zeta} + B\frac{\partial^3 \phi_1}{\partial \zeta^3} = 0, \tag{27}$$

where

$$A = -\frac{3}{4}V^3 q = -\frac{3q}{4p^{3/2}}, \qquad B = \frac{V^3}{2} = \frac{1}{2p^{3/2}}.$$

Using the expressions for p and q from Eqns. (14) and (15), we note that the coefficients A and B can be expressed explicitly as:

$$A = \frac{(1-\beta)}{\sqrt{\pi}\sqrt{\kappa - \frac{1}{2}}} \quad \frac{\Gamma(\kappa+1)}{\Gamma(\kappa+\frac{1}{2})}, \tag{28}$$

$$B = \frac{1}{2\left(1 + \frac{1}{\kappa - \frac{3}{2}}\right)^{3/2}}. \tag{29}$$

A is the coefficient of nonlinearity, which determines the steepness of the wave, while B is the coefficient of dispersion, responsible for wave broadening in Fourier space. Here, we see that the wave steepening is dependent both on the extent of superthermality of the electron distribution (represented by the κ parameter) and also on the density of the trapped electron distribution (represented by β), while wave width is dependent on κ alone. We note that $A \propto (1-\beta)$, and thus the term decreases linearly with β, vanishing at $\beta = 1$.

Limiting Case 1 - No superthermality If we assume there is no superthermality, that is, $\kappa \to \infty$, $A \to (1-\beta)/\sqrt{\pi}$, and $B \to 1/2$. This is in agreement with Ref. 22, Eqn. (14) therein, which defines a KdV-like evolutionary equation for trapped and free electrons in the context of a Maxwellian distribution.

Limiting Case 2 - No trapped electrons If we assume that there are no trapped electrons in the distribution, then $\beta \to 1$. We can see that this means the coefficient $q \to 0$, so consequently $A \to 0$, and we no longer have a Schamel KdV equation. In this case, returning to our fluid model (Eqns. (11) to (13)), the reductive perturbation method must be repeated with different stretching parameters, hence not yielding the $\phi^{3/2}$ term, but resulting in the standard KdV equation as obtained, for instance by Baluku et al. [25].

Figures 5 and 6 show the variation of A and B with superthermality. A is only weakly dependent on the κ parameter, increasing slightly at very low values of κ (high degree of superthermality). On the other hand, the dispersion coefficient B is strongly affected by superthermality. Increasing superthermality causes B to decrease significantly.

VI. SOLITON SOLUTION

Following Schamel [22], we seek a stationary solitary wave solution of Eqn. (27), and introduce $\xi = \zeta - u_0\tau$, where u_0 is the wave speed (in the reference frame) normalized by the ion acoustic sound speed c_s in an electron-ion plasma with Maxwellian electrons. We use the hyperbolic tangent method [27] as detailed in Ap-

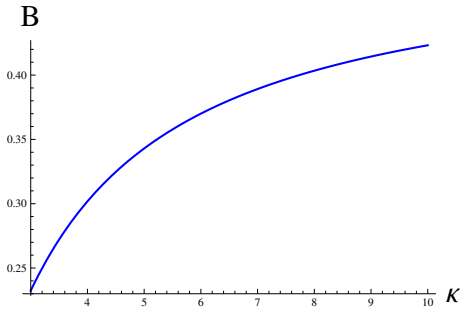

FIG. 6: (Color online). Plot of the coefficient B vs. κ.

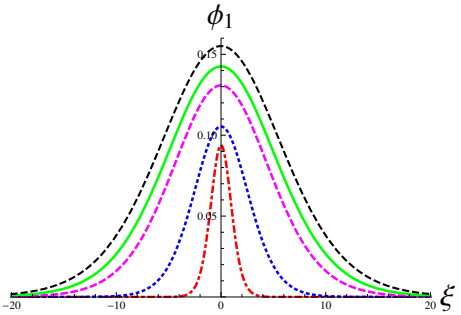

FIG. 7: (Color online). Plot of the solitary wave solution for different values of κ, based on (30). The dot-dashed (red) line is $\kappa = 1.6$, the dotted (blue) line is $\kappa = 2$, the dashed (mauve) line is $\kappa = 4$, the solid (green) line is $\kappa = 7$, and the dashed (black) line is $\kappa = 30$. Here we have taken $\beta = 0.5$ and $u_0 = 0.06$.

pendix A, and by imposing the following boundary conditions: $\phi_1 \to 0$, $\frac{d\phi_1}{d\xi} \to 0$, and $\frac{d^2\phi_1}{d\xi^2} \to 0$ as $\xi \to \pm\infty$, we find that the steady state can be expressed as

$$\phi_1 = \phi_m \,\mathrm{sech}^4\left(\xi/\Delta\right), \tag{30}$$

where

$$\phi_m = (15u_0/8A)^2, \tag{31}$$

$$\Delta = \sqrt{16B/u_0} \tag{32}$$

are the height and width of the solitary waves, respectively, moving with speed u_0. From Eqn. (31), we note that solitons can only have positive polarity, as is normal for ion acoustic solitons in a two-species plasma. In the limit as $\kappa \to \infty$, this is in agreement with Eqn. (20) of Ref. 28. For a given value of ϕ_m, we note that:

$$u_0 = \frac{8A}{15}\phi_m^{1/2}, \qquad \Delta = \sqrt{\frac{30B}{A\phi_m^{1/2}}}, \tag{33}$$

which coincides with Schamel [22], c.f. Eqns. (28) and (29) therein [29].

Figure 7 shows how the solitary wave solution varies with superthermality. We see that both the height and width of the wave are affected by changes in κ via the coefficients A and B. As superthermality increases (that is, the value of κ is decreased), the waves become smaller in amplitude and narrower. It should be emphasized that u_0 is the incremental soliton speed (i.e. in the wave frame), and the total soliton speed (i.e. in the laboratory frame) is found by adding u_0 and the κ-dependent phase speed V (detailed in Eqn. (23)). The true Mach number is then the total soliton speed divided by the phase speed. This is shown explicitly in Table I. In evaluating the information in Fig. (7) we need to be clear about what exactly has been kept constant. We stress that in the present calculations, we have assumed a constant incremental soliton speed u_0. Our results show qualitative agreement with those of Saini et al. [30], who used the Sagdeev pseudopotential technique to study arbitrary amplitude ion acoustic solitons in a two-species plasma with κ-distributed electrons. On the other hand, we see from the penultimate column of Table I, that fixed u_0 leads to the true Mach number increasing with enhanced superthermality. Other scenarios considered in the literature, often based on the Sagdeev technique, include, for instance, keeping either the true Mach number [25] or the total soliton speed $(u_0 + V)$ constant [31]. One may easily consider either of the above scenarios within the present Schamel-kappa formalism in which case one finds qualitative effects of increasing superthermality that are equivalent to those reported in the literature on solitons in plasmas in which the hot electrons are kappa-distributed.

TABLE I: Total soliton speed

κ	u_0	V	u_0/V	Total soliton speed (u_0+V)	True Mach no. $(1+u_0/V)$	ϕ_m
1.6	0.06	0.3015	0.1990	0.3615	1.1990	0.0937
2	0.06	0.5774	0.1039	0.6374	1.1039	0.1054
4	0.06	0.8451	0.0710	0.9052	1.0710	0.1308
7	0.06	0.9199	0.0652	0.9799	1.0652	0.1425
30	0.06	0.9829	0.0610	1.0429	1.0610	0.1551
∞	0.06	1.0000	0.0600	1.0600	1.06	0.1590

For example, the true Mach number is defined as

$$M_T = \frac{u_0 + V}{V},$$

where u_0 is the incremental soliton speed and V is the

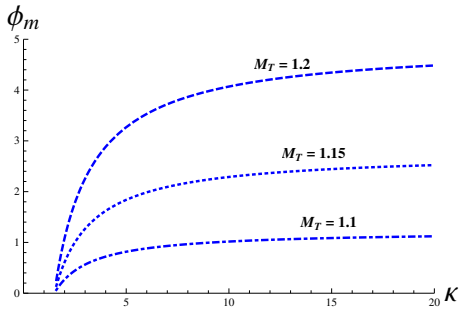

FIG. 8: Amplitude variation with kappa for 3 fixed Mach numbers ($M_T = 1.1, 1.15, 1.2$) at $\beta = 0.7$.

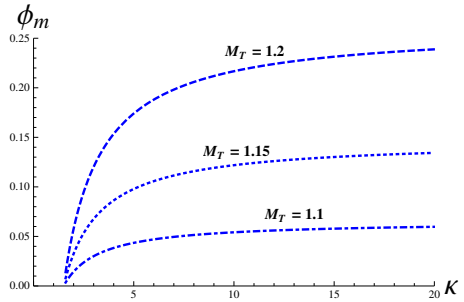

FIG. 9: Amplitude variation with kappa for 3 fixed Mach numbers ($M_T = 1.1, 1.15, 1.2$) at $\beta = -0.3$.

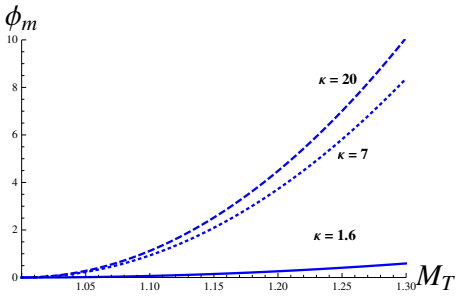

FIG. 10: Amplitude variation with Mach number for $\kappa = 1.6, 7, 20$ at $\beta = 0.7$.

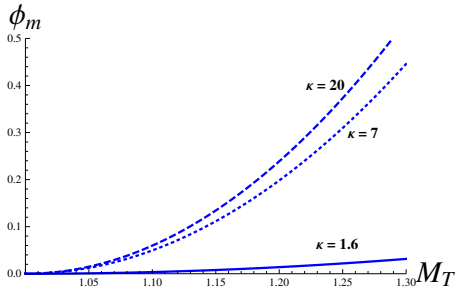

FIG. 11: Amplitude variation with Mach number for $\kappa = 1.6, 7, 20$ at $\beta = -0.3$.

phase speed given by (23). Rearranging, we find that

$$u_0 = V(M_T - 1).$$

Figures 8 and 9 show how the amplitude varies with κ when the true Mach number is held constant for the cases where $\beta = 0.7$ and $\beta = -0.3$, respectively. We note that the two figures are very similar, except that the soliton amplitudes are reduced by a factor of about 20 when switching from a weakly-trapped situation in the former to $\beta = -0.3$ in Fig. 9. Figures 10 and 11 show the amplitude variation with Mach number (M_T) when κ is kept constant, for the same values of β. In agreement with Baluku et al, [25], figure 3 therein, we note that ϕ_m increases with higher Mach numbers and reduces with increased superthermality. Again, we see a reduction in amplitude of about 20 between Figures 10 and 11.

Next we consider how the solitary wave varies with different proportions of electron trapping, while keeping u_0 fixed. From (31) and (28), we see that the amplitude of the wave is proportional to $1/(1-\beta)$ and thus particularly sensitive to changes in the β parameter as $\beta \to 1$, while being only weakly dependent on κ. Figure 12 provides visual confirmation of this, analagously to what has been seen in Figs. 8 to 11.

In Fig. 13, the solitary wave solution is plotted for different values of the β parameter. As β is decreased (that is, a smaller proportion of the electrons are trapped), the amplitude of the solitary wave is decreased and the width is unaffected. Our model does not allow for the situation where $\beta = 1$, as $A \to 0$ as $\beta \to 1$. For the purposes of comparison, we include a plot (Fig. 14) of the solitary wave solution for a standard KdV kappa superimposed on the Schamel KdV for the same value of κ. Interestingly, we note that the amplitude of a solitary wave with higher values of β, that is, above $\beta = 0.54$, is larger

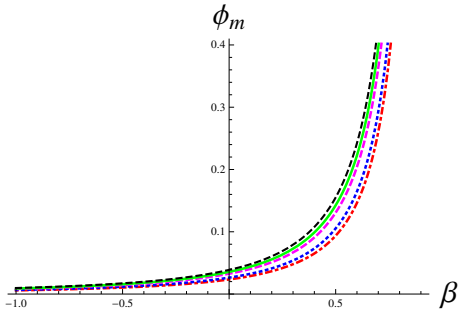

FIG. 12: (Color online). Plot of the solitary wave amplitude variation with β for different values of κ, based on (31). The dot-dashed (red) line is $\kappa = 1.6$, the dotted (blue) line is $\kappa = 2$, the dashed (mauve) line is $\kappa = 4$, the solid (green) line is $\kappa = 7$, and the dashed (black) line is $\kappa = 30$. Here we have taken $u_0 = 0.06$.

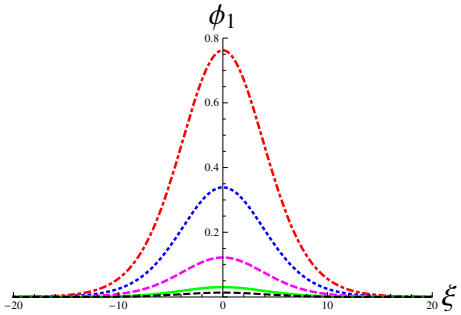

FIG. 13: (Color online). Plot of the solitary wave solution for different values of β, based on (30). The dot-dashed (red) line is $\beta = 0.8$, the dotted (blue) line is $\beta = 0.7$, the dashed (mauve) line is $\beta = 0.5$, the solid (green) line is $\beta = 0$ and the dashed (black) line is $\beta = -0.5$. Here we have taken $\kappa = 3$ and $u_0 = 0.06$.

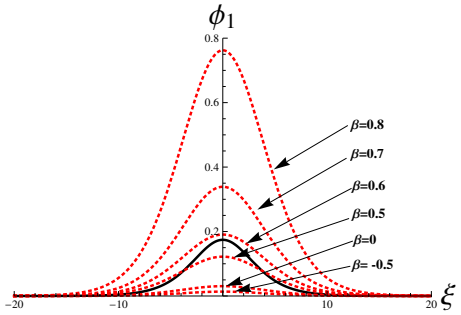

FIG. 14: (Color online). Plot of the solitary wave solution for standard KdV equation (see Appendix B) with $\kappa = 3$, shown as solid (black) line, superimposed on the Schamel KdV solitary wave for different values of β, shown in dotted (red) lines based on (30).

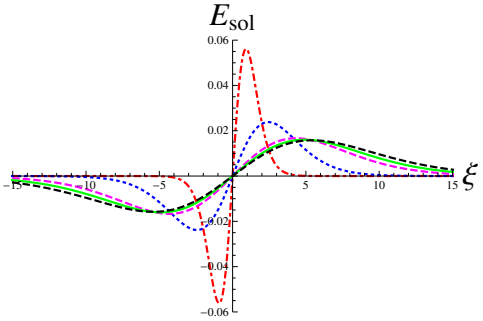

FIG. 15: (Color online). Plot of the solitary wave electric field magnitude for different values of κ, based on (34). The dot-dashed (red) line is $\kappa = 1.6$, the dotted (blue) line is $\kappa = 2$, the dashed (mauve) line is $\kappa = 4$, the solid (green) line is $\kappa = 7$, and the dashed (black) line is $\kappa = 30$. Here we have taken $\beta = 0.5$ and $u_0 = 0.06$.

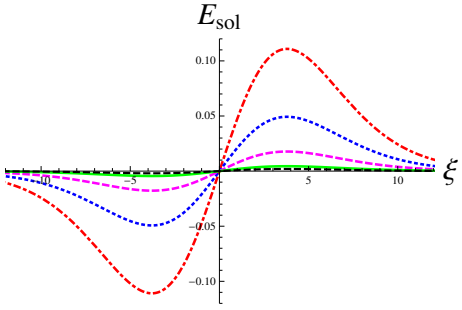

FIG. 16: (Color online). Plot of the solitary wave electric field magnitude for different values of β, based on (34). The dot-dashed (red) line is $\beta = 0.8$, the dotted (blue) line is $\beta = 0.7$, the dashed (mauve) line is $\beta = 0.5$, the solid (green) line is $\beta = 0$ and the dashed (black) line is $\beta = -0.5$. Here we have taken $\kappa = 3$ and $u_0 = 0.06$.

than that of a solitary wave in the standard kappa KdV description. Appendix B lays out the standard κ KdV solution alongside the κ Schamel solution.

The magnitude of the solitary wave's electric field can easily be found by taking the negative gradient of the solution, $E_{sol} = -\partial\phi_1/\partial\xi$. This gives:

$$E_{sol} = \frac{4\phi_m}{\Delta}\,\mathrm{sech}^4\left(\xi/\Delta\right)\tanh\left(\xi/\Delta\right), \tag{34}$$

where $\phi_m = (15u_0/8A)^2$ and $\Delta = \sqrt{16B/u_0}$ as before. Figures 15 and 16 show how the electric field varies with superthermality and the proportion of trapped electrons present. With increased superthermality we see the field becomes less localized with lower amplitude. As the proportion of trapped electrons is decreased (lower value of β), the magnitude of the electric field decreases.

VII. NUMERICAL RESULTS

We now trace the effects of the energy variation due to excess superthermality (via the κ parameter), and particle trapping (via β) on ion acoustic solitary waves, by numerically analysing ion acoustic solitary waves crossing an interface between two plasmas with different values of either κ or β. When a pulse representing an exact solution as given by Eqn. (27) passes to a plasma environment with different parameters, it must adapt by changing shape, becoming unstable, or changing speed.

The analytical results shown in Figs. 7 and 13 illustrate that higher superthermality (lower κ value) leads to narrower solitons with smaller amplitudes, and a lower proportion of trapped electrons (lower β value) leads to smaller amplitude solitons whose width remains unchanged, so we might expect the same trends to be dis-

played in the numerical results. Here we have analysed the propagation of ion acoustic solitary structures by a numerical integration of Eqn. (27) employing a Runge Kutta method with a time interval of 4×10^{-4}, and grid spatial size of 0.06. We retain as an intrinsic element in our code the dependence of the coefficients on the superthermality parameter κ and on the trapped electron population index β, as in our analytical model.

As a possible scenario in the dynamics, we choose to investigate the response of a stable pulse propagating in a weakly superthermal plasma, when it encounters a region with a strong deviation of hot electrons from thermal equilibrium or, alternatively, a region with a lower proportion of trapped electrons. To this end, we consider the soliton solution with $\kappa = 30$ and $\beta = 0.7$ as an initial condition. This same pulse is used as an initial condition in three simulations. In the first simulation, we integrate the Schamel KdV-like equation, (27), for the exact solution of $\kappa = 30$ and $\beta = 0.7$, with an incremental speed $u_0 = 0.12$, which confirms the stability of the pulse, as shown in subplot (a) of Figs. 17, 18 and 19.

Subsequently, we consider a lower value of κ, as shown in subplot (b) of the same figures, simulating the physical condition where a soliton propagating in a quasi-Maxwellian plasma enters a region with significantly higher proportions of superthermal electrons ($\kappa = 2$). We notice that the original pulse becomes taller and narrower, with an increased speed of approximately 0.19, while additionally two smaller solitary waves develop over time, travelling at a slower speed. A similar result in the context of electron acoustic waves was obtained by Sultana and Kourakis [32]. We speculate that the increase in the proportion of superthermal electrons causes the energy stored in the initial pulse to be distributed into energetically smaller pulses, while maintaining the delicate balance between nonlinearity and dispersion necessary for soliton stability.

In subplot (c) of Figs. 17, 18 and 19, we consider a lower value of the β parameter for the target plasma to see the effect of a wave propagating from one plasma environment into a region containing a lower proportion of trapped electrons. We can see that the original pulse becomes taller and narrower, with an increased speed of approximately 0.26 and a single weak extra solitary wave develops over time, travelling at a lower speed. Again it appears that the energy in the initial pulse has been redistributed and is sufficient to now form two pulses, each of lower energy than the original, even though, as in Fig. 17b, the amplitude of the leading pulse is larger than that of the original wave.

We note that in both (b) and (c) the original pulse becomes narrower and taller. At first sight that is counter-intuitive as we have seen above that pulses have smaller amplitudes in regions of increased excess superthermality or lower proportion of trapped electrons. However, the latter finding arose in a situation in which the incremental speed u_0 was constant. From Fig. 17 we have seen that the incremental speed changes dramatically at the interface between the two regions. In fact, u_0 has increased by about 50% in the low-kappa region in (b) and by 120% in the low β case in (c). Substituting these measured values for u_0 into (28 - 29) and (31 - 32) one finds predicted values of amplitudes and widths of the leading solitons that are consistent with those measured in the figure. It appears that energy conservation at the interface provides a constraint that leads to the value of u_0 increasing as observed, and to the spawning of one or more additional weak, slow solitons to mop up the balance of the energy arriving at the interface.

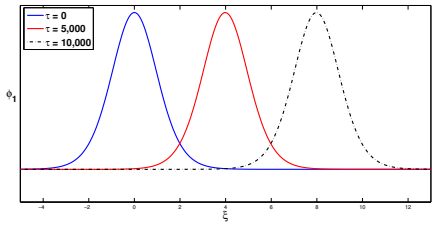

(a) Exact solution of initial condition with $\kappa = 30$, $\beta = 0.7$

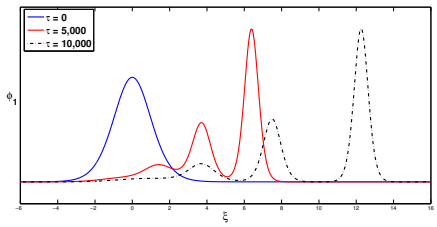

(b) Initial condition encounters $\kappa = 2$, $\beta = 0.7$ plasma

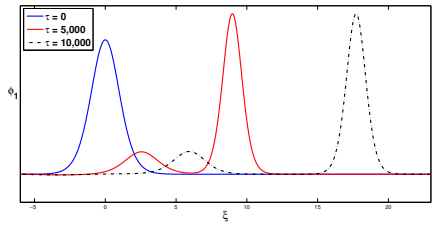

(c) Initial condition encounters $\kappa = 30$, $\beta = 0.4$ plasma

FIG. 17: (Color online). Evolution of electrostatic solitary structures based on Eqn. (27) and its solution, Eqn.(30). The exact solution of Eqn. (27) is considered as an initial condition in each subplot with $\kappa = 30$, $\beta = 0.7$, $u = 0.12$. This is propagating in (a) a quasi-Maxwellian plasma with high β parameter ($\kappa = 30$, $\beta = 0.7$); (b) a strongly nonthermal plasma with high β value ($\kappa = 2$, $\beta = 0.7$), and (c) a quasi-Maxwellian plasma with lower β value indicating a lower proportion of electron trapping ($\kappa = 30$, $\beta = 0.4$).

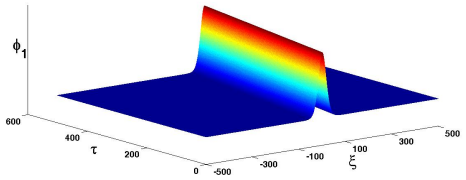

(a) Exact solution of initial condition with $\kappa = 30$, $\beta = 0.7$

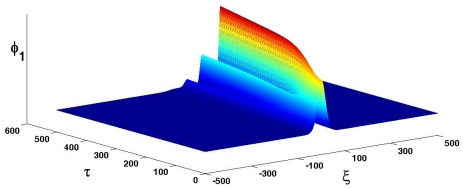

(b) Initial condition encounters $\kappa = 2$, $\beta = 0.7$ plasma

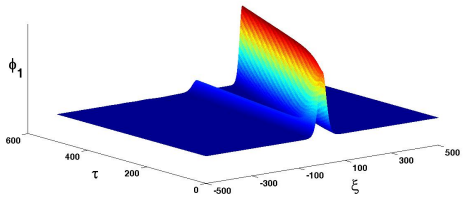

(c) Initial condition encounters $\kappa = 30$, $\beta = 0.4$ plasma

FIG. 18: (Color online). 3D plots showing the propagation of electrostatic solitary structures based on Eqns. (27) and (30) for similar conditions as in Fig. 17.

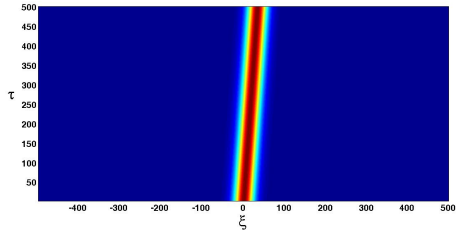

(a) Exact solution of initial condition with $\kappa = 30$, $\beta = 0.7$

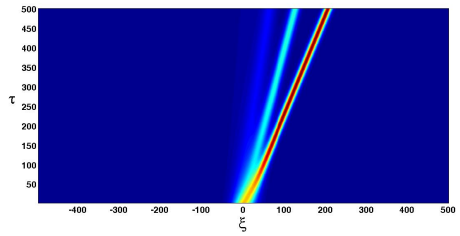

(b) Initial condition encounters $\kappa = 2$, $\beta = 0.7$ plasma

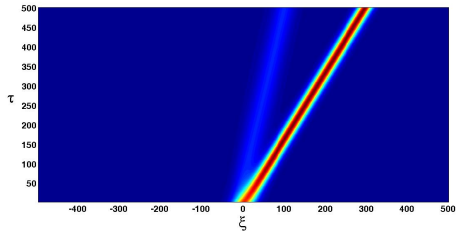

(c) Initial condition encounters $\kappa = 30$, $\beta = 0.4$ plasma

FIG. 19: (Color online). Propagation of electrostatic solitary structures based on Eqns. (27) and (30) in the space-time plan for similar conditions as in Figs. 17 and 18.

VIII. CONCLUSION

We have investigated solitary ion acoustic wave propagation in the presence of electron trapping and superthermality. A physically meaningful Schamel-like distribution has been developed. This Schamel-kappa distribution allows for the effects of trapped particles in the low energy part of the distribution, while including the usual enhanced non-Maxwellian tail, with an excess of superthermal particles, that is typical of a kappa distribution.

Using reductive perturbation theory, we have derived a Schamel equation, and its corresponding solitary wave solution.

At higher levels of superthermality the solitary wave amplitude decreases and wave structures become narrower. The corresponding electric field becomes more localized with much sharper peaks in conditions of high superthermality.

With higher proportions of free electrons, that is, a reduction in the value of the β parameter, the solitary wave amplitude decreases, becoming almost negligible for negative values of β; however, the width of the wave remains unchanged. The corresponding electric field amplitude also decreases as the proportion of trapped electrons decreases, whilst its spatial width is unchanged. We note that the amplitude of the wave is dependent on and particularly sensitive to changes in the β parameter.

Using numerical simulation, we find that the computed solution confirms the stability of the pulse. We also find that where a soliton propagating in a quasi-Maxwellian plasma enters a region of high superthermality, solitary waves change shape, becoming taller, narrower and faster, and give rise over time to two weak extra solitary pulses travelling at a lower speed. Also, when a soliton propagating in a quasi-Maxwellian plasma encounters a plasma with a higher proportion of free electrons, it changes shape, becoming narrower and faster and increasing in amplitude, and again over time, a single weak extra solitary wave forms, which travels at a lower speed.

Acknowledgments

GW gratefully acknowledges funding from DEL NI (Department of Employment and Learning Northern Ireland) in the form of a PhD studentship. MAH thanks the National Research Foundation of South Africa for partial support under Grant No. UID 85408, and acknowledges that opinions, findings, and conclusions or recommendations expressed in this publication are those of the authors, and that the NRF accepts no liability in this. The authors wish to thank Dr. Brian Reville for very helpful discussions regarding numerical analysis results. IK warmly acknowledges fruitful discussions and feedback from Hans Schamel (University Bayreuth, Germany).

Appendix A: Solitary wave solution of Eqn. (27)

The general solution of Eqn. (27) using the hyperbolic tangent (tanh) method [27], is detailed below. Let $\phi_1(\zeta,\tau)=\phi_1(\xi)$, where $\xi=\alpha(\zeta-u_0\tau)$. So Eqn. (27) becomes:

$$-\alpha u_0\frac{\partial\phi_1}{\partial\xi}+A\alpha\phi_1^{1/2}\frac{\partial\phi_1}{\partial\xi}+B\alpha^3\frac{\partial^3\phi_1}{\partial\xi^3}=0. \tag{A1}$$

Let $\phi_1^{1/2}=\psi$. Dividing across by α, integrating w.r.t. ξ, and assuming a soliton solution in which $\psi,\frac{\partial\psi}{\partial\xi},\frac{\partial^2\psi}{\partial\xi^2}\to 0$ as $\xi\to\pm\infty$ we get

$$-u_0\psi^2+\frac{2}{3}A\psi^3+2B\alpha^2\left[\left(\frac{\partial\psi}{\partial\xi}\right)^2+\psi\frac{\partial^2\psi}{\partial\xi^2}\right]=0. \tag{A2}$$

Using the transformation $y=\tanh(\chi)$, noting $\frac{\partial}{\partial\chi}=(1-y^2)\frac{d}{dy}$, and postulating a solution ψ such that: $\psi=\sum_n a_n y^n=a_0+a_1y+a_2y^2+...$, Eqn. (A2) becomes:

$$\begin{aligned}&-u_0\left(\sum_n a_n y^n\right)^2+\frac{2}{3}A\left(\sum_n a_n y^n\right)^3\\&+2B\alpha^2\left[\left((1-y^2)\frac{d}{dy}\sum_n a_n y^n\right)^2\right.\\&\left.+(1-y^2)\frac{d}{dy}(1-y^2)\frac{d}{dy}\sum_n a_n y^n\right]=0.\end{aligned} \tag{A3}$$

Truncating at $n=2$, a system of algebraic equations is found in orders of y, allowing us to solve for a_0,a_1,a_2, and α. We find (choosing a non-trivial solution for a_2 and a positive solution for α):

$$a_2=-\frac{30B\alpha^2}{A}, \tag{A4}$$

$$a_1=0, \tag{A5}$$

$$a_0=\frac{1}{A}\left[\frac{5u_0}{8}+20B\alpha^2\right], \tag{A6}$$

$$\alpha=\left(\frac{u_0}{16B}\right)^{\frac{1}{2}}. \tag{A7}$$

So $\psi=a_0+a_1y+a_2y^2$ is given by:

$$\psi=\frac{15u_0}{8A}\,\mathrm{sech}^2\left[\sqrt{\frac{u_0}{16B}}\,(\zeta-u_0\tau)\right]. \tag{A8}$$

But our soliton solution $\phi_1=\psi^2$ so finally:

$$\phi_1=\left(\frac{15u_0}{8A}\right)^2\mathrm{sech}^4\left[\sqrt{\frac{u_0}{16B}}\,(\zeta-u_0\tau)\right]. \tag{A9}$$

Appendix B: The standard KdV solitary wave solution compared with the Schamel for a κ distribution

The Schamel KdV Equation is given by Equation (27) above, rewritten below:

$$\frac{\partial\phi_1}{\partial\tau}+A\phi_1^{1/2}\frac{\partial\phi_1}{\partial\zeta}+B\frac{\partial^3\phi_1}{\partial\zeta^3}=0, \tag{B1}$$

where

$$\zeta=\epsilon^{1/4}\left(x-\frac{1}{\sqrt{p}}t\right),\qquad \tau=\epsilon^{1/4}t,$$

$$A=-\frac{3q}{4p^{3/2}},\qquad B=\frac{1}{2p^{3/2}},$$

$$p=\frac{\kappa-1/2}{\kappa-3/2},\quad q=\frac{8\sqrt{2/\pi}(\beta-1)\kappa\Gamma[\kappa]}{3(2\kappa-3)^{3/2}\Gamma[\kappa-1/2]}.$$

The solution for ϕ is $\phi\simeq\epsilon\phi_1$, where:

$$\phi_1=\phi_m\,\mathrm{sech}^4\left(\frac{\zeta-u_0\tau}{\Delta}\right), \tag{B2}$$

$$\phi_m=\left(\frac{15u_0}{8A}\right)^2,\quad \Delta=\sqrt{\frac{16B}{u_0}}. \tag{B3}$$

The electric field $E_{sol}=-\frac{\partial\phi_1}{\partial\zeta}$, which is:

$$E_{sol}=\frac{4\phi_m}{\Delta}\,\mathrm{sech}^4\left(\frac{\zeta-u_0\tau}{\Delta}\right)\tanh\left(\frac{\zeta-u_0\tau}{\Delta}\right). \tag{B4}$$

The standard KdV Equation is:

$$\frac{\partial\tilde{\phi}_1}{\partial T}+\tilde{A}\phi_1\frac{\partial\tilde{\phi}_1}{\partial Z}+\tilde{B}\frac{\partial^3\tilde{\phi}_1}{\partial Z^3}=0, \tag{B5}$$

where

$$Z=\epsilon^{1/2}\left(x-\frac{1}{\sqrt{p}}t\right), \qquad T=\epsilon^{3/2}t,$$

$$\tilde{A}=-\frac{3}{2}\sqrt{p}-\frac{r}{p^{3/2}}, \qquad \tilde{B}=\frac{1}{2p^{3/2}},$$

$$p=\frac{\kappa-1/2}{\kappa-3/2}, \qquad r=\frac{\kappa^2-1/4}{2(\kappa-3/2)^2}.$$

The solution for $\tilde{\phi}$ is $\tilde{\phi}\simeq\epsilon\tilde{\phi}_1$, where:

$$\tilde{\phi}_1=\tilde{\phi}_m\,\mathrm{sech}^2\left(\frac{Z-u_0T}{\tilde{\Delta}}\right), \tag{B6}$$

$$\tilde{\phi}_m=\frac{3u_0}{\tilde{A}}, \tag{B7}$$

$$\tilde{\Delta}=\sqrt{\frac{4\tilde{B}}{u_0}}. \tag{B8}$$

The electric field $\tilde{E}_{sol}=-\frac{\partial\tilde{\phi}_1}{\partial Z}$, which is:

$$\frac{2\tilde{\phi}_m}{\tilde{\Delta}}\,\mathrm{sech}^2\left(\frac{Z-u_0T}{\tilde{\Delta}}\right)\tanh\left(\frac{Z-u_0T}{\tilde{\Delta}}\right). \tag{B9}$$

[1] V. Vasyliunas, *J. Geophys. Res.*, **73**, 2839 (1968).
[2] M. A. Hellberg, R. L. Mace, T. K. Baluku, I. Kourakis and N. S. Saini, *Phys. Plasmas*, **16**, 094701 (2009).
[3] I. Kourakis, S. Sultana and M. A. Hellberg, *Plasma Phys. Cont. Fusion*, **54**, 124001 (2012).
[4] B.H. Mauk, D. G. Mitchell, R. W. McEntire, C. P. Paranicas, E. C. Roelof, D. J. Williams, S. M. Krimigis, A. Lagg, *J. Geophys. Res.*, **109**, A09S12 (2004).
[5] M. Hapgood, C. Perry, J. Davies and M. Denton, *Planet. Space Sci*, **59**, 618 (2011).
[6] G. Livadiotis and D. J. McComas, *J. Geophys. Res. Space Phys.*, **114**, A11 (2009).
[7] G. Livadiotis and D. J. McComas, *Astrophys. J.*, **741**, 88 (2011).
[8] H. Washimi and T. Taniuti, *Phys. Rev. Lett.*, **17**, 996 (1966).
[9] M.Q. Tran, *Physica Scripta*, **20**, 317 (1979).
[10] S. Sultana, G. Sarri and I. Kourakis, *Phys. Plasmas*, **19**, 012310 (2012).
[11] G. Williams and I. Kourakis, *Plasma Phys. Control. Fusion*, **55**, 055005 (2013).
[12] J.P. Lynov, P. Michelsen, H.L. Pecseli, J.J. Rasmussen, K. Saeki and V.A. Turikov, *Physica Scripta*, **20**, 328 (1979).
[13] M.V. Goldman, D.L. Newman and R.E. Ergun, *Nonlinear Proc. in Geophys.*, **10**, 37 (2003).
[14] P. Schippers, M. Blanc, N. André, I. Dandouras, G. R. Lewis, L. K. Gilbert, A. M. Persoon, N. Krupp, D. A. Gurnett, A. J. Coates, S. M. Krimigis, D. T. Young and M. K. Dougherty, *J. Geophys. Res.*, **113**, A07208 (2008).
[15] C. Cattell, C. Neiman, J. Dombeck, J. Crumley, J.Wygant, C.A. Kletzing, W.K. Peterson, F.S. Mozer, and M. André, *Nonlinear Proc. in Geophys.*, **10**, 13 (2003).
[16] R.E. Ergun, C.W. Carlson, J.P. McFadden, E.S. Mozer, G.T. Delory, W. Peria, C.C. Chaston, M. Temerin, I. Roth, L. Muschietti, R. Elphic, R. Strangeway, R. Pfaff, C.A. Cattell, D. Klumpar, E. Shelley, W. Peterson, E. Moebius and L. Kistler, *Geophys. Res. Lett.*, **25**, 2041 (1998).
[17] R.E. Ergun, L. Andersson, D.S. Main, Y.J. Su, C.W. Carlson, J.P. McFadden, and F.S. Mozer, *Phys. Plasmas*, **9**, 3685 (2002).
[18] L. Andersson, R.E. Ergun, D.L. Newman, J.P. McFadden, C.W. Carlson, and Y.J. Su, *Phys. Plasmas*, **9**, 3600 (2002).
[19] J.D. Moody and C.F. Driscoll, *Phys. Plasmas*, **2**, 4482 (1995).
[20] I.B. Bernstein, J.M. Green, M.D. Kruskal, *Phys. Rev.*, **108**, 546 (1957).
[21] H. Schamel, *Plasma Phys.*, **14**, 905 (1972).
[22] H. Schamel, *J. Plasma Phys.*, **9**, 377 (1973).
[23] F. Verheest and W. Hereman, *Physica Scripta*, **50**, 611 (1994).
[24] H. H. Pajouh and H. Abbasi, *Phys. Plasmas*, **15**, 103705 (2008).
[25] T.K. Baluku, M.A. Hellberg, I. Kourakis and N.S. Saini, *Phys. Plasmas*, **17**, 053702 (2010).
[26] N. Krall and A.W. Trivelpiece, *Principles of Plasma Physics*, McGraw-Hill, New York (1973).
[27] W. Malfliet and W. Hereman, *Phys. Scripta*, **54**, 563 (1996).
[28] M.G.M. Anowar and A.A. Mamun, *Phys. Plasmas*, **15**, 102111 (2008).
[29] Agreement achieved upon correcting a typing error therein, namely, $c=\frac{8}{15}\psi^{1/2}$, and formally taking into account the difference in notation.
[30] N. S. Saini, I. Kourakis and M. A. Hellberg, *Phys. Plasmas*, **16**, 062903 (2009).
[31] A. Danehkar, N. S. Saini, M. A. Hellberg and I. Kourakis, *Phys. Plasmas*, **18**, 072902 (2011).
[32] S. Sultana and I. Kourakis, *Eur. Phys. J. D.*, **66**, 100 (2012).